ISSN(Print) 2525-2321 ISSN(Online) 2572-8288

Vietnam Journal of CHEMISTRY

Volume 59, Number 4, August 2021

www.vjc.wiley-vch.de

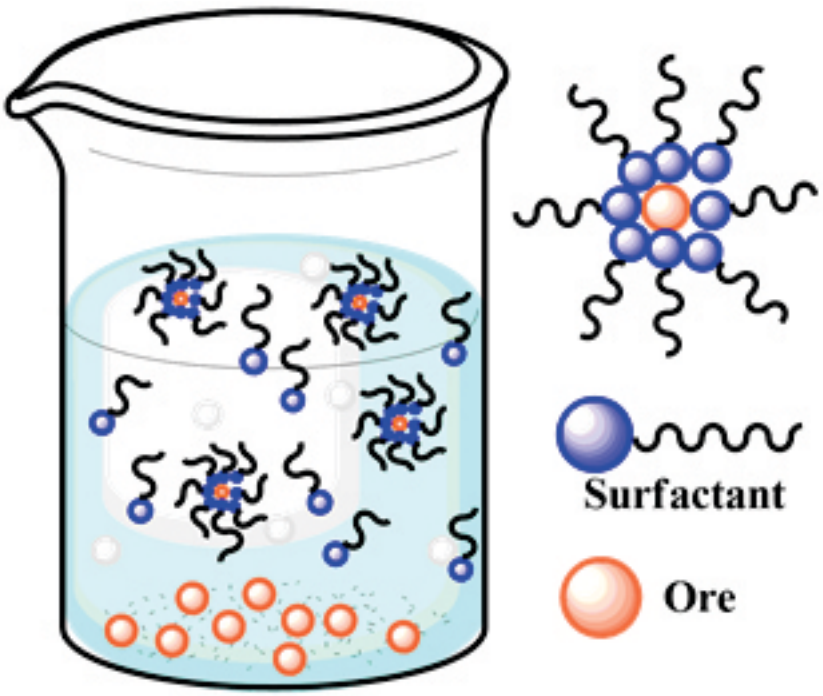

WILEY-VCH

VIETNAM ACADEMY
OF SCIENCE AND TECHNOLOGY

Cite this paper: Vietnam J. Chem., **2021**, *59(4)*, 431-439 Research article
DOI: 10.1002/vjch.202000152

Combination of photothermia and magnetic hyperthermia properties of Fe_3O_4@Ag hybrid nanoparticles fabricated by seeded-growth solvothermal reaction

Nguyen Thi Ngoc Linh[1,2*], Le The Tam[3], Ha Minh Nguyet[4], Ngo Thanh Dung[4], Nguyen Hoa Du[3], Le Thi Thanh Tam[4], Pham Hong Nam[5], Nguyen Dinh Vinh[1], Nguyen Thien Vuong[4], Ngo Dai Quang[6], Le Trong Lu[2,4*]

[1]*Thai Nguyen University of Sciences, Tan Thinh Ward, Thai Nguyen City 25000, Viet Nam*

[2]*Graduate University of Science and Technology, Vietnam Academy of Science and Technology, 18 Hoang Quoc Viet, Hanoi 10000, Viet Nam*

[3]*Vinh University, 182 Le Duan, Vinh City, Nghe An Province 46000, Viet Nam*

[4]*Institute for Tropical Technology, Vietnam Academy of Science and Technology, 18 Hoang Quoc Viet, Hanoi 10000, Viet Nam*

[5]*Institute of Materials Science, Vietnam Academy of Science and Technology, 18 Hoang Quoc Viet, Hanoi 10000, Viet Nam*

[6]*Vietnam national Chemical Group, 2 Pham Ngu Lao street, Hoan Kiem, Hanoi 10000, Viet Nam*

Submitted September 1, 2020; Revised May 28, 2020; Accepted June 1, 2021

Abstract

In this work, the monodisperse Fe_3O_4@Ag core-shell hybrid nanoparticles (NPs) with an average size of 16.0 nm have been successfully fabricated by the seeded-growth method in the organic solvent. The influence of the molar ratios of $AgNO_3$/OLA on the formation of hybrid NPs has been investigated in detail to find the optimal conditions for the synthesis of the desired Fe_3O_4@Ag hybrid NPs. The hydrophobic Fe_3O_4@Ag hybrid NPs were successfully transferred into the water using poly (maleic anhydride-alt-1-octadecene) (PMAO). The PMAO coated Fe_3O_4@Ag nanoparticles were well dispersed and stable in water over a wide range of pH from 2 to 11 as well as reasonable electrolyte concentration. The Fe_3O_4@Ag magneto-plasmonic design can efficiently combine magnetic hyperthermia into an effective bimodal thermo-therapy.

Keywords. Fe_3O_4@Ag, core-shell, magnetic hyperthermia, plasmonic photothermal, thermo-therapy.

1. INTRODUCTION

In recent years, nanomaterials have been widely used in biomedicine such as cancer diagnosis and treatment.[1, 2] Among various efforts to develop new drugs and treatment methods for cancer, thermal therapy has been emerging as a potential alternative to all current approaches due to its promisingly high efficiency without negative side effects. Subsequently, thermal treatment using nanoparticles has attracted more and more attention from researchers. This field of study aims to fabricate novel nanostructures that can convert electromagnetic energy or/and light energy into heat with maximum productivity and minimum possible risks to living bodiesby shortening exposure time, lowering exciting electromagnetic frequencies, or using longer-wavelength laser, etc. The reported materials including magnetic and noble metallic nanomaterials still exhibit certain drawbacks when being used independently.[3–5]

Recent studies have shown that the combination of magnetic and plasmonic properties into a single unit would integrate the advantages of the two components as well as enhance their relative functions.[6] Currently, the utilization of magneto-plasmonic hybrid NPs for biomedical purposes focuses mainly on Fe_3O_4/Au nanostructures.[7] The studies on Fe_3O_4/Au hybrid NPs for magnetic hyperthermia and photothermia have obtained some remarkable results.[8,9] The benefit of this material in therapy is that it can selectively destroy tumor cells with few side effects for healthy cells under the impact of light or magnetic activities or both of them

simultaneously.[10] However, the fabrication of Fe_3O_4/Au nanostructures for this purpose is at a very high cost, making it difficult to be applied to many patients. Therefore, reducing the cost of products but still achieving the goal of treatment are urgent requirements. Fe_3O_4/Ag hybrid NPs are a promising candidate to replace Fe_3O_4/Au hybrid NPs in cancer treatment by magneto-photothermal therapy.[11] However, high-quality studies on Fe_3O_4/Ag hybrid NPs in this field are still rather scarce. Especially, the growth mechanism and the role of experimental parameters on the development of hybrid nanoparticle morphology are still unclear. As proved in previously published studies, the magnetic properties of Fe_3O_4 core can help improve magnetic hyperthemia[11,12] and the magnetic resonance imaging (MRI),[13] while Ag component exhibits photothermal heating into the hybrid structure.[14] Therefore, integrating the strong points of the magnetic hyperthermia of Fe_3O_4 and the plasmonic photothermal effects of Ag into a hybrid nanostructure for cancer treatment is a promising and brand-new approach.

In this paper, we designed multifunctional Fe_3O_4@Ag hybrid nanostructures with plasmonic and magnetic properties using the seeded-growth method.[15] The Fe_3O_4 seeds were prepared by thermal decomposition of $Fe(acac)_3$ precursor which is safer and cheaper than $Fe(CO)_5$. Despite its popularity in previous studies, $Fe(CO)_5$ is a highly toxic and expensive reactant.[16] The effect of $AgNO_3$/OLA molar ratios on the morphology and dispersity of Fe_3O_4@Ag hybrid NPs was investigated to optimize the conditions for the formation of Fe_3O_4@Ag core-shell nanostructure. The Fe_3O_4@Ag hybrid NPs were transferred into the water using PMAO polymer. The as-synthesized hybrid nanostructure can efficiently combine the magnetic hyperthermia of Fe_3O_4 core with the photo-thermal response of silver shells like the dual hyperthermia system. The obtained Fe_3O_4@Ag hybrid NPs open up a promising potential for cancer treatment.

2. MATERIALS AND METHODS

2.1. Chemicals

All chemicals used in the fabrication process were of analytical grade (purchased from Sigma-Aldrich Ltd, Singapore) including Iron(III) acetylacetonate ($Fe(acac)_3$), silver nitrate ($AgNO_3$), oleic acid (OA), oleylamine (OLA), 1-octadecanol (OCD-ol), poly (maleic anhydride-alt-1-octadecene) (PMAO), 1-octadecene (ODE), chloroform ($CHCl_3$), absolute ethanol (C_2H_5OH) and *n*-hexane (C_6H_{14}). They were used directly without any further purification.

2.2. Preparation of materials

2.2.1. Synthesis of Fe_3O_4 nanoparticles

Fe_3O_4 nanoparticles were fabricated by the thermal decomposition method in organic solvents as reported in our previous work.[17] In a typical synthesis, $Fe(acac)_3$ (673 mM), OA (744 mM), OLA (744 mM), and OCD-ol (300 mM) were mixed and stirred magnetically in a 100-mL three-neck flask containing 40 mL of ODE under nitrogen flow. First, the reaction mixture was de-gassed at room temperature within 30 min before being heated up gradually to 100 ^oC to remove water for about 30 min. After that, the solution was refluxed at 200 ^oC for another 30 min. Finally, the system temperature was adjusted to 295 ^oC with a steady rate of 5 ^oC min^{-1} and then maintained for 60 min. The obtained mixture was left to cool down naturally to room temperature, then washed with ethanol, centrifuged, and lastly re-dispersed in *n*-hexane solvent. The collected NPs were dried before being physicochemically characterized.

2.2.2. Synthesis of Fe_3O_4@Ag hybrid nanoparticles

The Fe_3O_4@Ag hybrid NPs were synthesized using the seeded-growth method. In brief, 6 mL of OLA and 0.3 g of OCD-ol were dissolved in 40 mL ODE in a three-neck flask. 5 mL *n*-hexane containing 0.1 g of the purified Fe_3O_4 NPs (seeds) (section 2.2.1) was injected into the mixture while continuously stirred under nitrogen flow. A certain quantity of $AgNO_3$ was added to obtain solutions with different molar ratios of $AgNO_3$/OLA = 0.15:1, 0.3:1 and 0.45:1, labeled as FA0.15, FA0.3, and FA0.45, respectively. The reaction mixture was heated to 80 ^oC and kept at this temperature for 30 min to remove *n*-hexane. Afterward, the system was heated to 200 ^oC at a rate of 5 ^oC min^{-1}, and then refluxed for 60 min before being cooled down to room temperature. The as-synthesized Fe_3O_4@Ag hybrid NPs were purified from free Ag nanoparticles and excess ligands before being characterized. The control Ag NPs were synthesized under the same conditions without the appearance of Fe_3O_4 seeds.

2.2.3. Phase transfer Fe_3O_4@Ag hybrid NPs into water

According to a recently developed procedure, PMAO polymer can support the transfer of the hydrophobic Fe_3O_4@Ag hybrid NPs into the

aqueous solvent.[18] In short, a solution of 50 mg of Fe_3O_4@Ag NPs dispersed in 10 mL of chloroform was mixed with 2 mL of chloroform containing 0.5 g PMAO by magnetically stirring for 60 min. The mixture was then dried at normal conditions before being dissolved into 10 mL of diluted NaOH solution under ultrasonication. For supernatant removal and purification, the hybrid NPs were repeatedly centrifuged at 12000 rpm and redispersed in water. The final product was dispersed in 10 mL of water.

2.3. Materials characterization

Structural investigations of materials were recorded on a Siemens D5005 diffractometer at room temperature (300K) with CuK_α radiation (λ = 1.5418 Å). The particle size and shape were determined by using a transmission electron microscope (TEM, JEOL JEM-1010, Japan). The average size and the size distribution of nanoparticles were analyzed according to TEM images using ImageJ software. Infrared and UV-Vis spectra were obtained by the FT-IR NEXUS 670 (Nicolet, USA) and the UV-Vis spectrophotometer (Jasco V-670, Japan). The elemental composition of the fabricated materials was checked using an energy dispersive X-ray spectrometer (EDS, Jeol 6490-JED 2300). The magnetic properties of the materials at room temperature were measured using a vibrating sample magnetometer (VSM) with a field of up to 10 kOe. Dynamic light scattering (DLS) measurements and stability of the magnetic fluids were examined by a Zetasizer (Malvern, UK).

2.4. Magnetic and photo-induced heating mode measurements

To investigate the magnetic and/or photo-induced heating efficiency of Fe_3O_4@Ag hybrid nanoparticles, the energy conversion experiments were carried out under an alternating magnetic field of 80 Oe with a frequency of 178 kHz created by a commercial generator UHF-20A and infrared light having wavelength of 532 nm with a maximum power density of 2.5 W/cm^2. In a typical measurement, pure water was used as the control.

3. RESULTS AND DISCUSSION

3.1. Synthesis and characterization of Fe_3O_4@Ag hybrid NPs

The synthesis of Fe_3O_4@Ag hybrid nanoparticles was depicted in figure 1. In the early stage, the Fe_3O_4 NPs were prepared by the decomposition of the $Fe(acac)_3$ precursor in ODE solvent at high temperature. The second step was the preparation of Fe_3O_4@Ag hybrid NPs by the seeded-growth method using Fe_3O_4 as seeds, $AgNO_3$ precursor, OCD-ol as reducing agent, and OLA as surfactant and ligand. In solution, Ag-oleylamine complex was formed and then reduced by OCD-ol to generate Fe_3O_4@Ag core-shell hybrid NPs.

The morphology of NPs was observed using a transmission electron microscope (TEM). Figure 2 showed the TEM images and size distribution chart of Fe_3O_4 seeds and Fe_3O_4@Ag hybrid NPs which were synthesized at different molar ratios of $AgNO_3$/OLA. The results indicated that the Fe_3O_4 particles were spherical, monodisperse, uniform in size and shape with an average size of 8.5±0.9 nm (figure 2a). It can be seen that the morphology of Fe_3O_4@Ag hybrid NPs depends on the molar ratios of precursors and surfactants ($AgNO_3$/OLA). In detail, with $AgNO_3$/OLA = 0.15:1 (figure 2b) the obtained core-shell structure was not uniform including both small and large spherical particles.

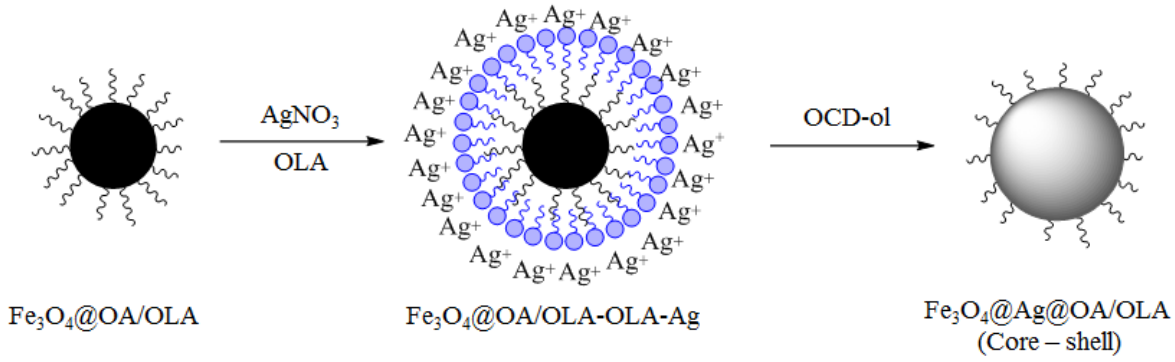

Figure 1: Schematic illustration of the formation process of Fe_3O_4@Ag hybrid NPs

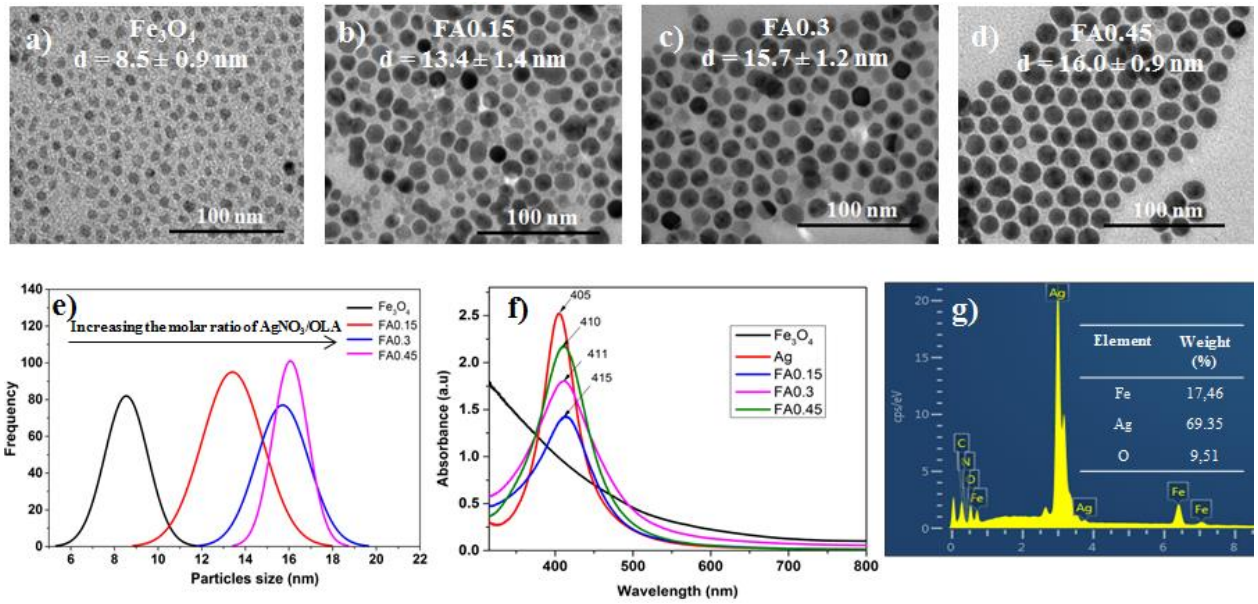

Figure 2: TEM images and the corresponding size distribution histograms of Fe_3O_4, Ag, and Fe_3O_4@Ag hybrid NPs (a-e); UV-Vis absorption spectra of Fe_3O_4, Ag, and Fe_3O_4@Ag hybrid NPs (f); EDS data of FA0.45 sample (g)

The small NPs could be original Fe_3O_4 NPs or Fe_3O_4 coated with a very thin Ag shell. The large particles with an average diameter of 13.4±1.4 nm were supposed to be Fe_3O_4@Ag core-shell hybrid NPs. The uneven shell thickness may be due to the low Ag precursor concentration. Nonetheless, when the $AgNO_3$/OLA ratio was 0.3:1, the free Fe_3O_4 particles were not observed, however, the Fe_3O_4@Ag hybrid NPs were not uniform in shape and size (figure 2c). Markedly, at the molar ratio of $AgNO_3$/OLA = 0.45:1, the formed Fe_3O_4@Ag hybrid NPs were uniform in size and shape with the average size of 16.0±0.9 nm (figure 2d). By continuously raising the ratios of $AgNO_3$/OLA, the size of Fe_3O_4@Ag hybrid NPs significantly increased (figure 2e). These results can be explained as follows: Through the growth reaction, the Ag atoms first started depositing on the surface of Fe_3O_4 seeds. Then, the positions with the presence of Ag atoms became more active, facilitating a large amount of Ag to continue depositing. Hence, the Ag shell was formed gradually through the formation of Ag nanocrystals. However, when the concentration of the Ag precursor was low (the molar ratio of $AgNO_3$/OLA was low), both active sites with many Ag atoms and vacant positions on the surface of the Fe_3O_4 cores would simultaneously appear, resulting in the competition and dominance of the Ostwald ripening effect. This led to an uneven formation of the Ag shell.[19]

The formation of Fe_3O_4@Ag hybrid nanostructures was also confirmed through the UV-Vis absorption spectra. As presented in figure 2f, in the wavelength range of 300-800 nm, the Fe_3O_4 NPs had no absorption peak, while Ag NPs showed a surface plasmon resonance (SPR) peak at 405 nm, the Fe_3O_4@Ag hybrid NPs showed peaks in the wavelength range of 410-415 nm. The SPR peaks of Fe_3O_4@Ag were red-shifted with different degrees compared to those of Ag NPs. This change was due to the local dielectric effect according to Mie theory.[20] Moreover, the presence of an SPR band in the UV-Vis spectrum of Fe_3O_4@Ag hybrid nanostructures was also an indicator of the silver shell layer formation on the Fe_3O_4, totally in agreement with the results observed from TEM image. In addition, the energy-dispersive X-ray spectroscopy (EDS) analysis of a representative sample FA0.45 further confirmed the coexistence of Fe, Ag, and O elements in the hybrid structure (figure 2g). Altogether, these results demonstrated that Fe_3O_4@Ag hybrid NPs with core-shell structure had been successfully fabricated. Due to its high uniformity, the FA0.45 sample was used to further study the properties of Fe_3O_4@Ag hybrid nanostructure.

Figure 3 showed the X-ray diffraction patterns of Fe_3O_4, Ag, and Fe_3O_4@Ag hybrid nanostructures. Obviously, the diffraction peaks at 2-theta angles of 30.16°, 35.49°, 43.01°, 53.78°, 57.21°, and 62.73° corresponding to the reflection planes of (2 2 0), (3 1 1), (4 0 0), (4 2 2), (5 1 1), and (4 4 0) indicated the *fcc* inverse-spinel structure of Fe_3O_4 (JCPDS no. 19-0629). The XRD pattern of Ag NPs matched the

face-centered cubic (*fcc*) structure with peaks at the positions of 38.21°, 43.61°, and 64.21°, corresponding to (1 1 1), (2 0 0), and (2 2 0) crystal planes of Ag standard pattern (JCPDS no. 004-0783). For Fe_3O_4@Ag core-shell structure (FA0.45 sample), it can be only seen the characteristic peaks of Ag structure, while the typical peaks of Fe_3O_4 structure were not observed. A plausible explanation for this phenomenon was that Fe_3O_4 cores were completely coated by Ag shell (as observed by TEM image - figure 2d).

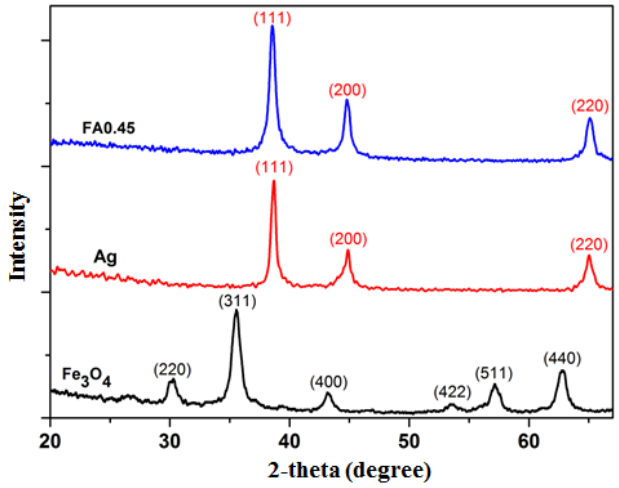

Figure 3: XRD patterns of Fe_3O_4 NPs (black), Ag NPs (red), and Fe_3O_4@Ag hybrid NPs (blue)

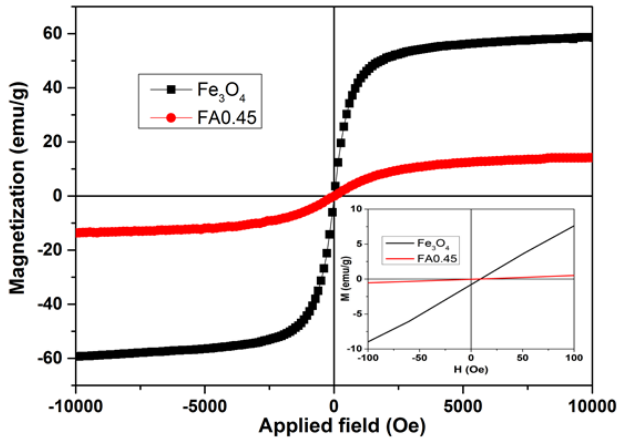

Figure 4: Magnetization curves of Fe_3O_4 NPs and Fe_3O_4@Ag hybrid NPs

The magnetic properties of materials were analyzed using vibrating sample magnetometry (VSM). The results showed that the synthesized Fe_3O_4 NPs and Fe_3O_4@Ag hybrid NPs were superparamagnetic at room temperature (figure 4). The saturation magnetization of Fe_3O_4 particles was 58.7 emu/g, higher than that of FA0.45 (15.2 emu/g). Additionally, the coercivity (H_c) decreased from 10 Oe for Fe_3O_4 seeds to 0 Oe for hybrid nanoparticles. This result could be explained by the existence of the non-magnetic Ag component in the hybrid structure.

3.2. Fe_3O_4@Ag hybrid NPs are coated by PMAO

The Fe_3O_4@Ag hybrid NPs were covered by a hydrophobic layer of OA and OLA, such that they can be dispersed in non-polar organic solvents. For biological application purposes, they must be dispersible in water. Therefore, FA0.45 sample was transferred into the water by the amphiphilic PMAO polymer. It is clear that the original hybrid nanoparticles were dispersible in *n*-hexane and non-dispersible in water. After being coated by PMAO, the surface of the hybrid nanoparticles became hydrophilic, thus making them well-dispersed in water (figure 5a). The TEM image of PMAO encapsulated Fe_3O_4@Ag hybrid NPs was shown in figure 5b. As illustrated, the hybrid nanoparticles were well isolated without any agglomeration.

To apply Fe_3O_4@Ag hybrid NPs in living systems, it is crucial to evaluate their stability. For this reason, a dynamic light scattering (DLS) was performed to measure the hydrodynamic diameters of Fe_3O_4@Ag NPs in water. As demonstrated in figure 5c, the sample FA0.45 showed only one peak at 25.85 nm with the width of the narrow bottom, implying that the PMAO-encapsulated particles were relatively uniform with an average size of 25.85 nm. Besides, the fluids of hybrid NPs were high stability with zeta potential value of -42.5 mV (figure 5d).

The PMAO-capped hybrid NPs were well-dispersed and stable in the solutions of NaCl at a concentration up to 250 mM. However, the higher concentration of NaCl (for example, 275 mM) led to the aggregation and precipitation of the nanoparticles (figure 6a). Likewise, the colloid of the PMAO-modified hybrid NPs was stable within a wide range of pH from 2 to 11. The precipitation appeared at a low pH of 1 (figure 6b).

The FT-IR spectra of OA/OLA-capped and PMAO-modified hybrid NPs could be evidence of the PMAO occurrence on the surface of the Fe_3O_4@Ag hybrid NPs (figure 7a). For both samples, there were characteristic peaks, indicating the presence of CH_2 groups in OA, OLA, and PMAO molecules. In the sample after phase transfer, there was a band at 3441 cm^{-1} that could be assigned to the oscillation of hydroxyl groups in water

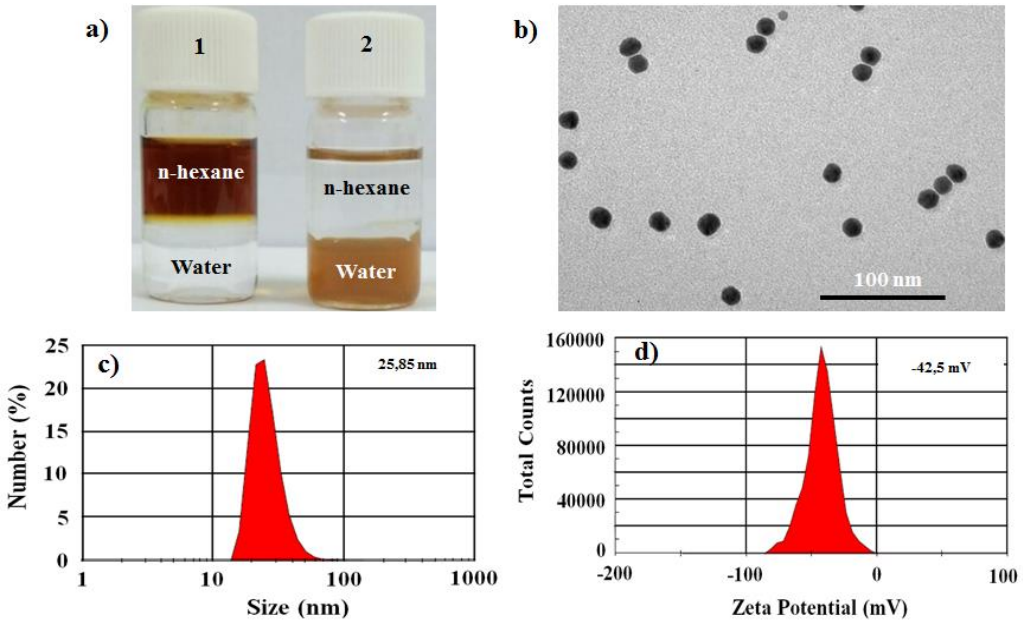

Figure 5: Photographs of Fe_3O_4@Ag hybrid NPs before (1) and after (2) the surface modification by PMAO (a), TEM images of PMAO encapsulated Fe_3O_4@Ag hybrid NPs (b), hydrodynamic size distribution (c) and zeta potential (d) of PMAO encapsulated Fe_3O_4@Ag hybrid NPs

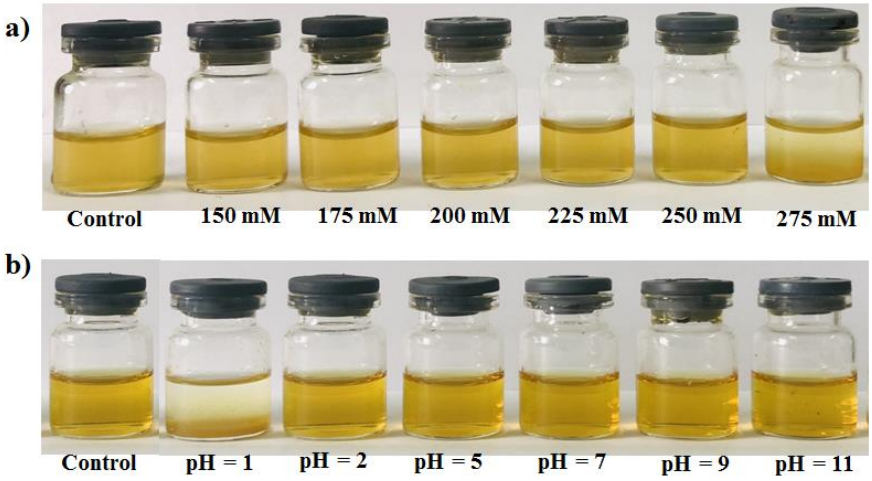

Figure 6: Images of the PMAO encapsulated Fe_3O_4@Ag hybrid NPs solution in water at different NaCl concentrations (a) and different pH values (b)

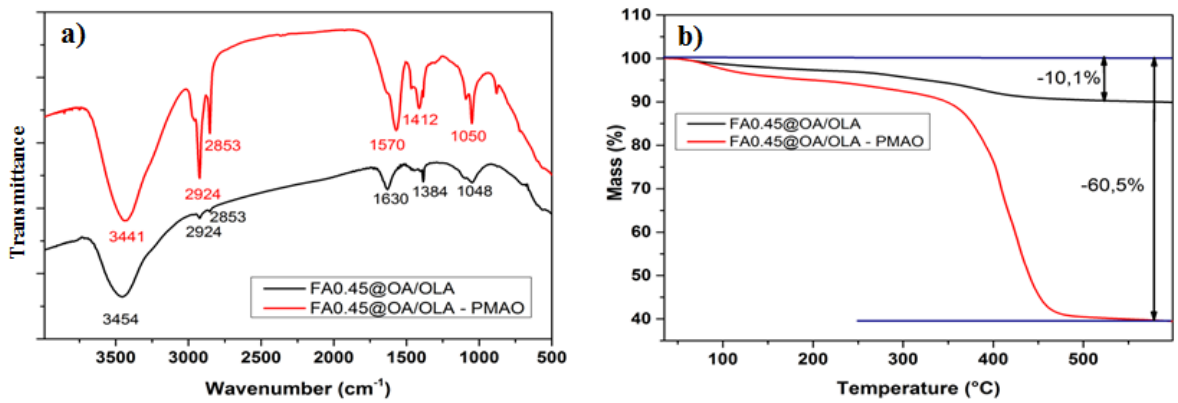

Figure 7: FT-IR spectra (a) and TGA scans (b) of OA/OLA and of PMAO encapsulated Fe_3O_4@Ag hybrid NPs

molecules absorbed by the PMAO layer encapsulating the hybrid NPs. Meanwhile, the spectrum of the sample before PMAO surface modification showed a band in the range of 1384-1500 cm^{-1} and a peak at 1630 cm^{-1} that can be attributed to the carboxylate group of OA and the amine group of the OLA, respectively. Nevertheless, a strong peak at 1570 cm^{-1} represented the ionized carboxylic acid created by the open of the anhydride rings of PMAO molecules in the alkaline medium, once again detecting the presence of PMAO on the hybrid particle surface. No doubt that these carboxylic groups helped to enhance the aqueous dispersion ability of hybrid NPs capped by PMAO.

Investigation of TGA diagram (Figure 7b) was consistent with the above observation. Particularly, the sample before phase transfer (FA0.45@OA/OLA) had lost approximately 10 % by weight when the temperature raised from 70 to 550 °C, corresponding to the evaporation of organic solvent absorbed onto the surface of NPs and the decomposition of surfactants (OA and OLA). Whilst, the sample after phase transfer (FA0.45@OA/OLA-PMAO) showed a significant decrease of 60 % in weight within the same temperature range. The weight loss had resulted from the water evaporation (≈ 10 %), the decomposition of OA/OLA (≈ 10 %), and the destruction of PMAO (≈ 40 %).

3.3. The magneto-photo-thermal conversion efficiency of Fe_3O_4@Ag hybrid NPs

The heating effect of the Fe_3O_4@Ag hybrid NPs was investigated with the FA0.45 sample after phase transfer (FA0.45@OA/OLA-PMAO) at a concentration of 0.2 mg/mL Fe. Experiments were conducted under 3 conditions: (i) Magnetic hyperthermia (MHT) at a magnetic field of 80 Oe and frequency of 178 kHz, (ii) Photothermal therapy (PTT) under 532 nm laser at a power density of 0.3 W/cm^2, and (iii) Combined magnetic field and laser (MHT + PTT) at the same conditions.

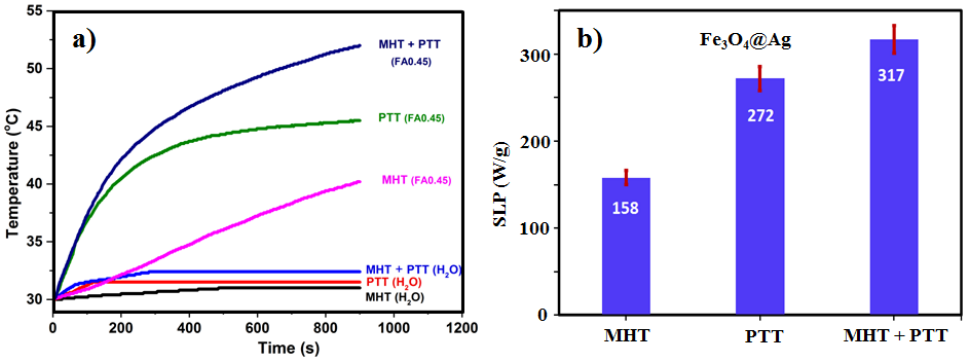

Figure 8: (a) Heating curves for the Fe_3O_4@Ag hybrid NPs solution and H_2O under MHT alone (80 Oe, 178 kHz), PTT alone (532 nm, 0.3 W/cm^2) and bimodal MHT+PTT (same parameters), and (b) SLP values vs. heating curves obtained from (a) for the Fe_3O_4@Ag hybrid NPs solution

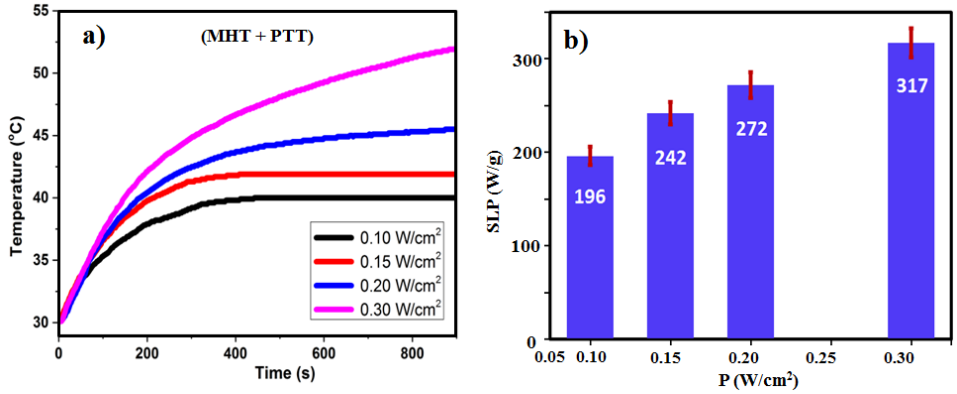

Figure 9: Heating curves (a), and SLP values (b) for the Fe_3O_4@Ag hybrid NPs solution under the combination of a magnetic field of 80 Oe and 178 kHz, and 532 nm laser for values of the power density ranging from 0.1 to 0.3 W/cm^2

As shown in figure 8, the temperature elevations of FA0.45 sample under three heating modalities MHT, PTT, and (MHT + PTT) were 10.2, 15.5, and 22.0 °C, respectively. The specific loss power (SLP) values were 158, 272, and 317 W/g, respectively, after 900 s of the experiment. Pure water as the

control showed only a negligible temperature increase (1.0-2.5 ºC) under MHT, PTT, and (MHT + PTT), indicating that the temperature rise of the hybrid solution was due to the heating effect of the Fe_3O_4@Ag hybrid NPs. The results also suggested that the heating effect of the Fe_3O_4@Ag NPs could be greatly enhanced under the dual magnetic/photo heating mode (MHT + PTT).

To further investigate the heating effect of Fe_3O_4@Ag hybrid NPs, the heating efficiency of FA0.45 sample was studied under the combined exposure to the constant magnetic field of 80 Oe and 178 kHz, and varying irradiation of 532 nm laser at different power density from 0.1 to 0.3 W/cm^2 (figure 9). The results showed that the temperature change induced by the hybrid sample during the measurement. When laser power density increased from around 0.1 to 0.3 W/cm^2, the temperature elevation increased from 10 to 22 ºC and SLP values increased from 196 to 317 W/g, respectively, after 900 s of the treatment. In addition, we observed that in order to reach the expected temperatures (42-46 ºC), the magnetic field of 80 Oe and 178 kHz required a power density of 0.15 W/cm^2 (figure 9a), while in the absence of a magnetic field, the laser irradiation of 0.3 W/cm^2 was needed (PTT FA0.45, Figure 8a). Obviously, the combination of magnetic field and laser irradiation could achieve therapeutic temperatures while minimizing exposure intensities. Undoubtedly, the research results showed the potential application of the Fe_3O_4@Ag hybrid NPs in cancer treatment.

4. CONCLUSIONS

The Fe_3O_4@Ag core-shell hybrid NPs with an average size of 16.0 nm were successfully fabricated in organic solvent using the seeded-growth method. The uniformity of hybrid nanostructures depended on the molar ratio of $AgNO_3$/OLA. The hydrophobic Fe_3O_4@Ag hybrid NPs were successfully transferred into the water using poly (maleic anhydride-alt-1-octadecene) (PMAO). The PMAO coated Fe_3O_4@Ag nanoparticles were well dispersed and stable in water over a wide range of pH from 2 to 11 as well as reasonable electrolyte concentration. The Fe_3O_4@Ag hybrid nanostructure could act as dual hyperthermia agents. The heating effect of the hybrid NPs could be greatly enhanced when the magnetic and plasmonic modalities were applied simultaneously. All things considered, this study demonstrated a highly applicable potential of Fe_3O_4@Ag hybrid nanostructure for dual magnetic/photo heating in cancer treatment.

Acknowledgment. *This research is funded by the Ministry of Education and Training (MOET) under grant number B2020-TDV-04 (N.H.Du).*

REFERENCES

1. A. A. Yaqoob, H. Ahmad, T. Parveen, A. Ahmad, M. Oves, I. M. I. Ismail, H. A. Qari, K. Umar, M. N. M. Ibrahim. Recent advances in metal decorated nanomaterials and their various biological applications: A review, *Front. Chem.*, **2020**, *8*, 341-363.
2. S. Rajkumar, M. Prabaharan. Multi-functional core-shell Fe_3O_4@Au nanoparticles for cancer diagnosis and therapy, *Colloids Surfaces B Biointerfaces*, **2019**, *174*, 252-259.
3. S. Gul, S. B. Khan, I. U. Rehman, M. A. Khan, M. I. Khan. A Comprehensive review of magnetic nanomaterials modern day theranostics, *Front. Mater.*, **2019**, *6*, 179-183.
4. M. Kim, J. H. Lee, J. M. Nam. Plasmonic photothermal nanoparticles for biomedical applications, *Adv. Sci.*, **2019**, *6*, 1900471-1900493.
5. D. Jaque, L. M. Maestro, B. Rosal, P. H. Gonzalez, A. Benayas, J. L. Plaza, E. M. Rodrigueza, J. G. Solea. Nanoparticles for photothermal therapies, *Nanoscale*, **2014**, *6*, 9494-9530.
6. H. Kakwere, M. E. Materia, A. Curcio, M. Prato, A. Sathya, S. Nittia, T. Pellegrino. Dually responsive gold-iron oxide heterodimers: Merging stimuli-responsive surface properties with intrinsic inorganic material features, *Nanoscale*, **2018**, *10*, 3930-3944.
7. T. T. Nguyen, F. Mammeri, S. Ammar. Iron oxide and gold based magneto-plasmonic nanostructures for medical applications: A review, *Nanomaterials*, **2018**, *8*, 149-177.
8. S. Shams, M. Ghazanfari, C. Schmitz-Antoniak. Magnetic-plasmonic heterodimer nanoparticles: Designing contemporarily features for emerging biomedical diagnosis and treatments, *Nanomaterials*, **2019**, *9*, 97-135.
9. J. G. Ovejero, I. Morales, P. Presa, N. Mille, J. Carrey, M. A. Garcia, A. Hernando, and P. Herrasti. Hybrid nanoparticles for magnetic and plasmonic hyperthermia, *Phys. Chem. Chem. Phys.*, **2018**, *20*, 24065-24073.
10. A. Espinosa, M. Bugnet, G. Radtke, S. Neveu, G. A. Botton, C. Wilhelm, A. A. Hassan. Can magneto-plasmonic nanohybrids efficiently combine photothermia with magnetic hyperthermia?, *Nanoscale*, **2015**, *7*, 18872-18877.
11. Q. Ding, D. Liu, D. Guo, F. Yang, X. Pang, R. Che, N. Zhou, J. Xie, J. Sun, Z. Huang N. Gu. Shape-controlled fabrication of magnetite silver hybrid nanoparticles with high performance magnetic hyperthermia, *Biomaterials*, **2017**, *124*, 35-46.

12. M. E. F. Brollo, J. M. O. Henao, R. L. Ruiz, D. Muraca, C. S. B. Dias, K. R. Pirota, M. Knobel. Magnetic hyperthermia in brick-like Ag@Fe_3O_4 core-shell nanoparticles, *J. Magn. Magn. Mater.*, **2016**, *397*, 20-27.
13. Y. Mao, P. Yi, Z. Deng, J. Ge. Fe_3O_4-Ag heterostructure nanocrystals with tunable Ag domains and magnetic properties, *CrystEngComm*, **2013**, *15*, 3575-3581.
14. H. Wang, J. Shen, G. Cao, Z. Gai, K. Hong, P. R. Debata, P. Banerjeea, S. Zhou. Multifunctional PEG encapsulated Fe_3O_4@silver hybrid nanoparticles: Antibacterial activity, cell imaging and combined photothermo/chemo - therapy, *J. Mater. Chem. B*, **2013**, *1*, 6225-6234.
15. J. Jiang, H. Gu, H. Shao, E. Devlin, G. C. Papaefthymiou, J. Y. Ying. Bifunctional Fe_3O_4-Ag heterodimer nanoparticles for two-photon fluorescence imaging and magnetic manipulation, *Adv. Mater.*, **2008**, *20*, 4403-4407.
16. E. Fantechi, A. G. Roca, B. Sepulveda, P. Torruella, S. Estrade, F. Peiro, E. Coy, S. Jurga, N. G. Bastus, J. Nogues, V. Puntes. Seeded growth synthesis of Au-Fe_3O_4 heterostructured nanocrystals: rational design and mechanistic insights, *Chem. Mater.*, **2017**, *29*, 4022-4035.
17. L. T. Lu, N. T. Dung, L. D. Tung, C. T. Thanh, O. K. Quy, N. V. Chuc, S. Maenosonoe, N. T. K. Thanh. Synthesis of magnetic cobalt ferrite nanoparticles with controlled morphology, monodispersity and composition: The influence of solvent, surfactant, reductant and synthetic conditions, *Nanoscale*, **2015**, *7*, 19596-19610.
18. N. T. Dung, N. V. Long, L. T. T. Tam, P. H. Nam, L. D. Tung, Nguyen X. Phuc, L. T. Lu, N. T. K. Thanh. High magnetisation, monodisperse and water-dispersible CoFe@Pt core/shell nanoparticles, *Nanoscale*, **2017**, *9*, 8952-8961.
19. N. T. T. Trang, T. T. Thuy, K. Higashimine, D. M. Mott, S. Maenosono. Magnetic-plasmonic FePt@Ag core-shell nanoparticles and their magnetic and SERS properties, *Plasmonics*, **2013**, *8*, 1177-1184.
20. P. Singh, C. Upadhyay. Size selectivity of magnetite core - (Ag/Au) shell nanoparticles for multimodal imaging applications, *Mater. Res. Express*, **2017**, *4*, 105401-105409.

Corresponding authors: **Le Trong Lu**
Institute for Tropical Technology
Vietnam Academy of Science and Technology
18, Hoang Quoc Viet Street, Cau Giay, Hanoi 10000, Viet Nam
E-mail: ltlu@itt.vast.vn.

Nguyen Thi Ngoc Linh
Thai Nguyen University of Sciences
Tan Thinh Ward, Thai Nguyen City, Thai Nguyen province 25000, Viet Nam
E-mail: linhntn@tnus.edu.vn.

WILEY-VCH

VJC | Vietnam Journal of CHEMISTRY

Pages 417-535, Volume 59, Number 4, August 2021

TABLE OF CONTENTS

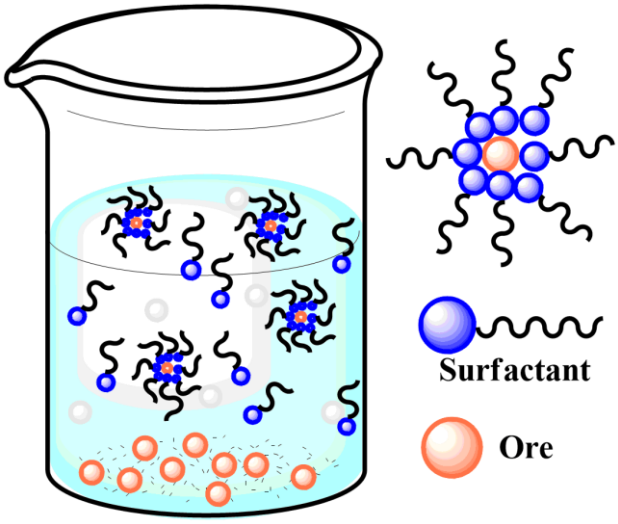

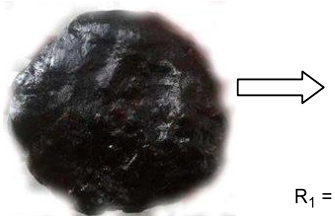

Lisotrigona furva Propolis

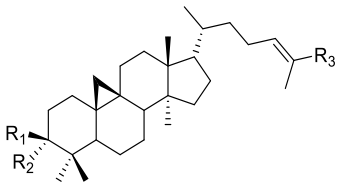

$R_1 + R_2$ =O, R_3 = Me: Cycloartenone (**1**)

R_1 = OH, R_2 = H, R_3 = Me: Cycloartenol (**2**)

R_1 = OH, R_2 = H, R_3 = CHO: (24*E*)-3β-hydroxycycloart-24-en-26-al **(3)**

$R_1 + R_2$ =O, R_3 = COOH: Mangiferonic acid (**4**)

R_1 = OH, R_2 = H, R_3 = Me: Mangiferolic acid (**5**)

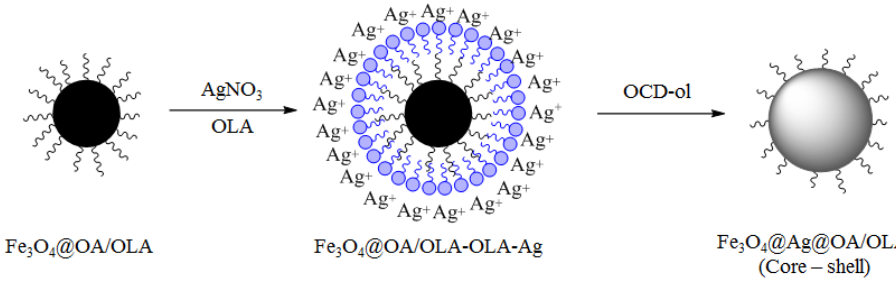

Schematic illustration of the formation process of Fe_3O_4@Ag hybrid NPs

440

Preparation of $CaCO_3$ nano and microparticles from phosphogypsum of Dinh Vu DAP plant, Viet Nam

Dang Ngoc Phuong*, Ngo Kim Chi, Tran Le Minh, Hoang Huu Luat, Chu Quang Truyen, Tran Dai Lam

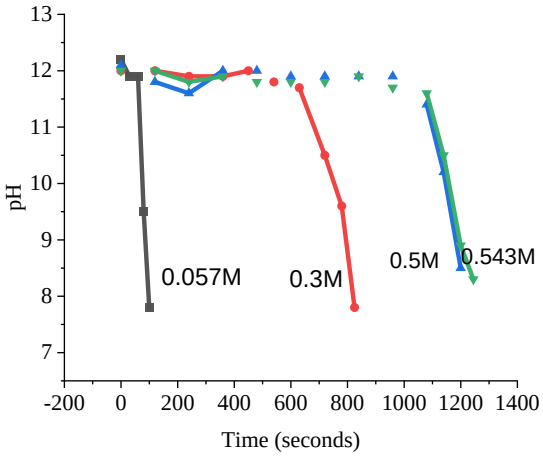

pH curves recoded during aeration process (44 °C, aeration rate of 90 ml/min)

446

Investigation of acute toxicity of composite Cu_2O NPs/Diatomite on white mice

Dinh Thi Nga, Dang Thi Thuy Nhung, Tran Thi Thanh Ngoc, Phan Dinh Tuan*, Nguyen Quoc Hien

Natural diatomite

Cu_2O nano/diatomite

451

Triterpenoids and steroids from the lichen *Ramalina peruviana* Arch

Huynh Bui Linh Chi*, Nguyen Thi Thuy Linh, Le Hong Hanh, Phan Hoang Linh, Pham Nguyen Kim Tuyen, Nguyen Tan Phat, Nguyen Thi Anh Tuyet

Ramalina peruviana

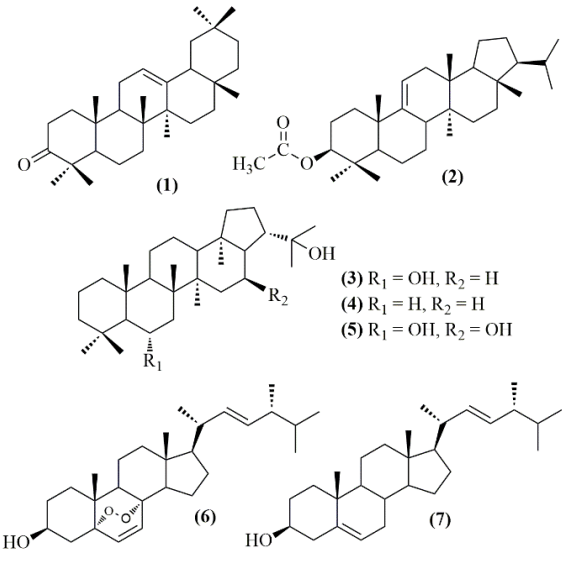

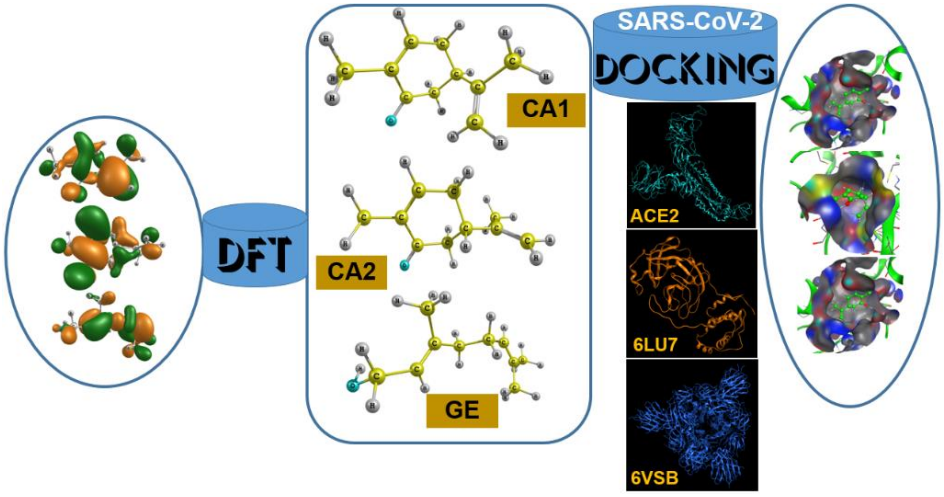

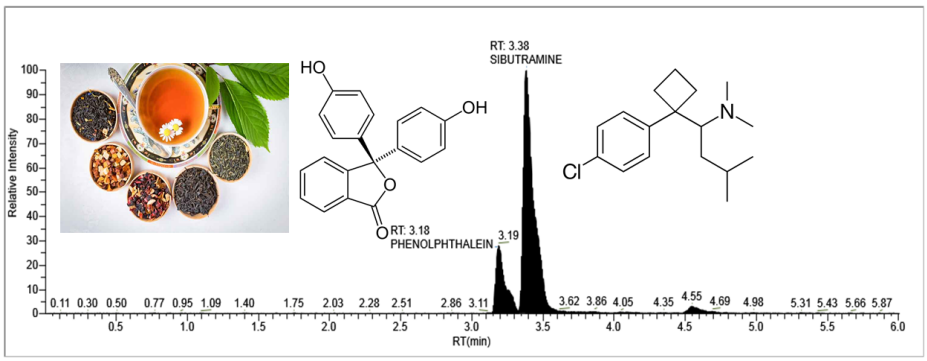

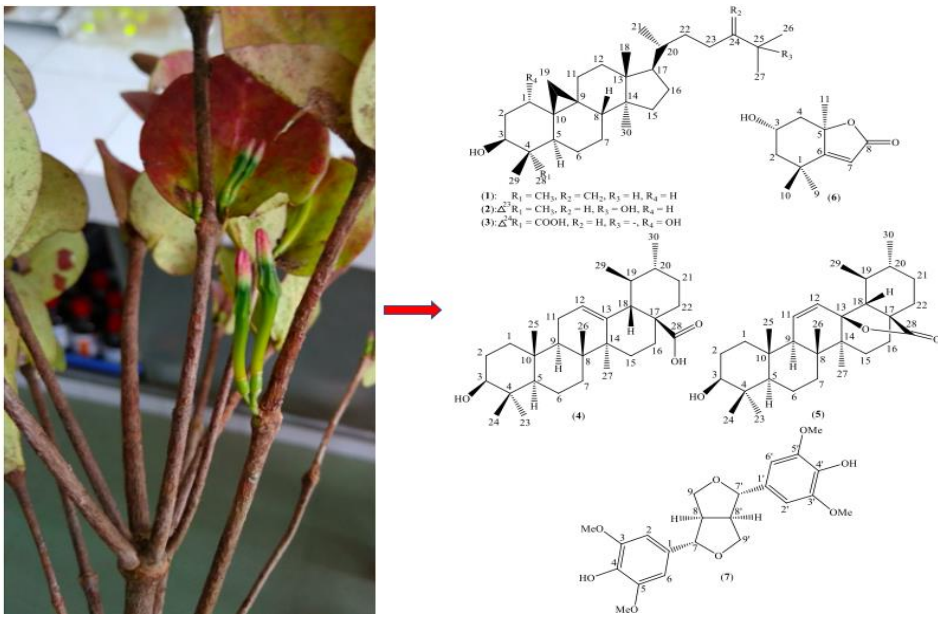

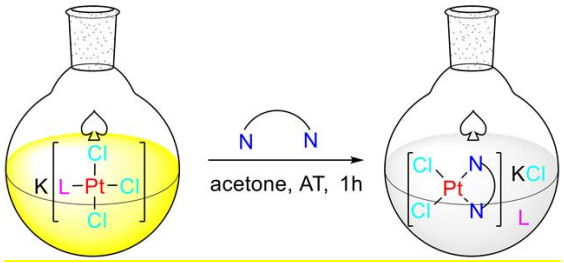

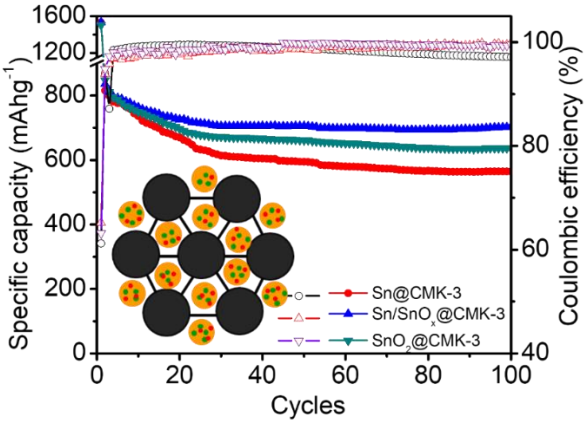

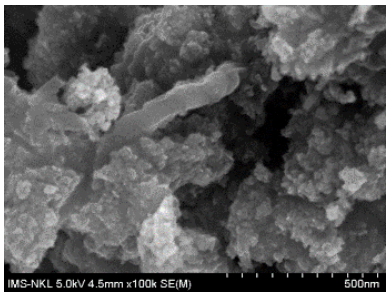

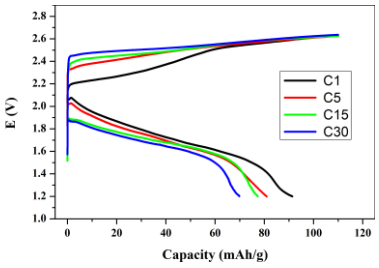

SEM image and the charge - discharge curves of the MnO$_2$/CNTs composite

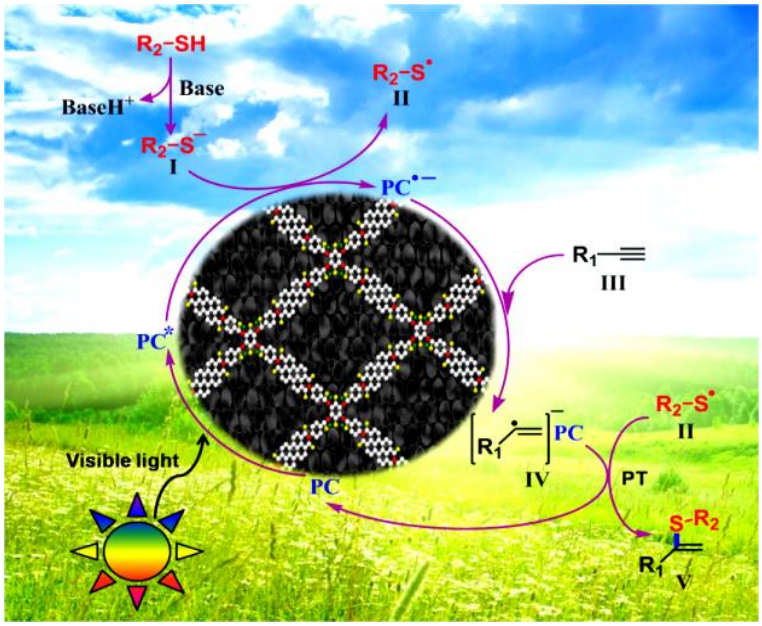

511

Synthesis of new 3-(hydroxymethyl)-2-phenyl-2,3 dihydroquinolinone and *in-silico* evaluation of COVID-19 main protease inhibitor

Amaladoss Nepolraj*, Vasyl I Shupeniuk, Manisekar Sathiyaseelan, Nagamuthu Prakash

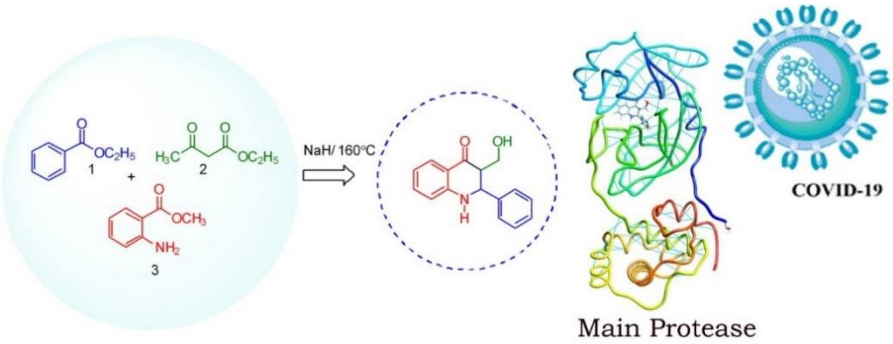

522

A new meroterpene lactone and a new alkyl amino alcohol from the Vietnamese marine sponge *Hippospongia fistulosa* Lendenfeld, 1889

Dan Thi Thuy Hang, Do Thi Trang, Pham Hai Yen, Nguyen Thi Cuc, Duong Thi Dung, Bui Huu Tai, Nguyen Xuan Nhiem, Phan Van Kiem*

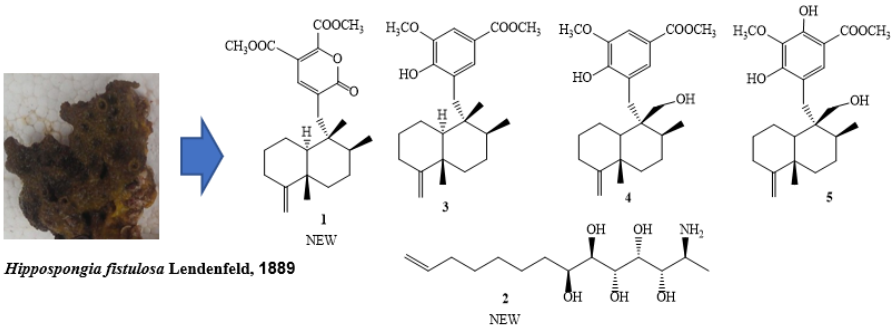

527

Effect of substituents on complex stability and characteristics of C_{sp2}-H···O/S and O/S-H···S/Se hydrogen bonds in the systems of monosubstituted selenoformaldehyde with H_2O and H_2S

Nguyen Thi Thanh Cuc, Le Thi Tu Quyen, Ho Cong Hau, Nguyen Thi Dieu Cam, Vu Thi Ngan, Nguyen Tien Trung*

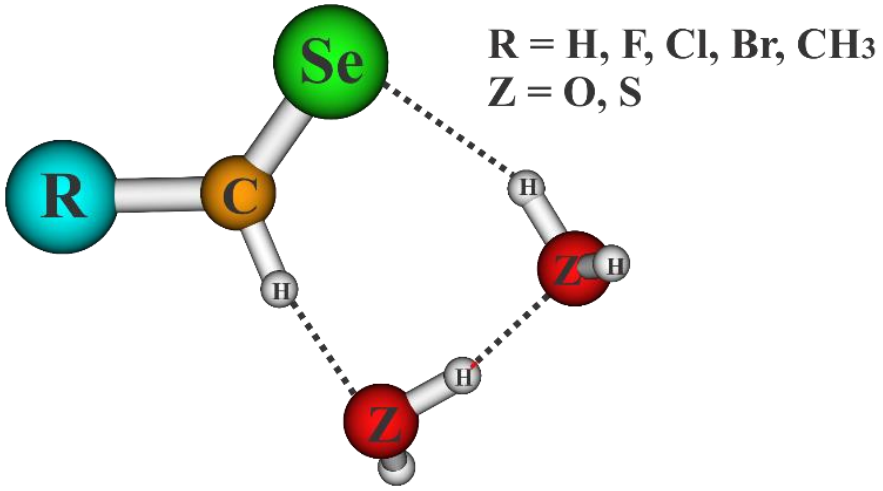

A noticeable role of H_2O relative to H_2S in blue shift of C_{sp2}-H stretching frequencies and stabilization of complexes

